Journal of Luminescence 131 (2011) 429–432

Contents lists available at ScienceDirect

Journal of Luminescence

journal homepage: www.elsevier.com/locate/jlumin

Energy transfer in $Y_3Al_5O_{12}:Ce^{3+}$, Pr^{3+} and $CaMoO_4:Sm^{3+}$, Eu^{3+} phosphors

Jiahua Zhang [a,*], Lei Wang [a,b], Ye Jin [a], Xia Zhang [a], Zhendong Hao [a], Xiao-jun Wang [c]

[a] Key Laboratory of Excited State Processes, Changchun Institute of Optics, Fine Mechanics and Physics, Chinese Academy of Sciences, 3888 Eastern South Lake Road, Changchun 130033, China

[b] Graduate School of Chinese Academy of Sciences, Beijing 100039, China

[c] Department of Physics, Georgia Southern University, Statesboro, GA 30460, USA

ARTICLE INFO

Available online 15 September 2010

Keywords:
YAG:Ce^{3+},Pr^{3+}
LED phosphors
Energy transfer

ABSTRACT

Non-radiative energy transfers (ET) from Ce^{3+} to Pr^{3+} in $Y_3Al_5O_{12}:Ce^{3+}$, Pr^{3+} and from Sm^{3+} to Eu^{3+} in $CaMoO_4:Sm^{3+}$, Eu^{3+} are studied based on photoluminescence spectroscopy and fluorescence decay patterns. The result indicates an electric dipole–dipole interaction that governs ET in the LED phosphors. For Ce^{3+} concentration of 0.01 in YAG:Ce^{3+}, Pr^{3+}, the rate constant and critical distance are evaluated to be 4.5×10^{-36} $cm^6\,s^{-1}$ and 0.81 nm, respectively. An increase in the red emission line of Pr^{3+} relative to the yellow emission band of Ce^{3+}, on increasing Ce^{3+} concentration is observed. This behavior is attributed to the increase of spectral overlap integrals between Ce^{3+} emission and Pr^{3+} excitation due to the fact that the yellow band shifts to the red spectral side with increasing Ce^{3+} concentration. In $CaMoO_4:Sm^{3+}$, Eu^{3+}, Sm^{3+}–Eu^{3+} transfer occurs from $^4G_{5/2}$ of Sm^{3+} to $^5D_0$ of Eu^{3+}. The rate constant of 8.5×10^{-40} $cm^6\,s^{-1}$ and the critical transfer distance of 0.89 nm are evaluated.

1. Introduction

White light-emitting diodes (LEDs) have attracted much interest in recent years for their significant potentials in solid-state lighting of next generation. At present the main strategy for producing white LEDs is to combine blue and/or near UV (NUV) LED with phosphors. The combination of blue LED with the yellow emitting $Y_3Al_5O_{12}:Ce^{3+}$ (YAG:Ce^{3+}) phosphor is a general way to produce white light. YAG:Ce^{3+} can effectively absorb blue light and subsequently emit yellow light, originating from the transition from the lowest 5d state to $^2F_{5/2}$ and $^2F_{7/2}$ ground states of Ce^{3+} [1,2]. However, YAG:Ce^{3+} has relatively weak emission in the red spectral region, leading to low color rendering of white LEDs. To enhance the red component, Mueller-Mach et al. [3] added Pr^{3+} to YAG:Ce^{3+} and consequently observed a sharp red line at about 608 nm, originating from $^1D_2\rightarrow{}^3H_4$ transition of Pr^{3+}, meaning the performance of energy transfer (ET) from Ce^{3+} to Pr^{3+} in YAG. Subsequently, YAG:Ce^{3+}, Pr^{3+} attracted many investigations [4–7].

The combination of a NUV LED with RGB phosphors is another alternative to produce white light, which may provide a high color rendering and stable color point against forward current. Among the RGB phosphors, red-emitting phosphors are scarce at present. Eu^{3+} doped $CaMoO_4$ has been investigated as a potential red-emitting phosphor because it exhibits more stable physical and chemical properties than the well-known red phosphor $Y_2O_2S:Eu^{3+}$. The red emission is originated from $^5D_0\rightarrow{}^7F_2$ transition of Eu^{3+} and the NUV excitation performs at around 395 nm through $^7F_0\rightarrow{}^5L_6$ absorption of Eu^{3+}. Some investigations on enhancing the luminescence intensity of $CaMoO_4:Eu^{3+}$ were reported by introducing Li^+, Na^+, K^+ and Bi^{3+} ions into the phosphor [8–10]. In our previous work [11], we added Sm^{3+} to $CaMoO_4:Eu^{3+}$ to generate additional NUV excitation line at 405 nm, originating from $^6H_{5/2}\rightarrow{}^4K_{11/2}$ absorption of Sm^{3+} based on the performance of ET from Sm^{3+} to Eu^{3+}. The significance of the transfer is to extend the excitation lines in the spectral range 390–410 nm so as to take advantage of all spectral components of the NUV LED excitation source. Energy transfer from Sm^{3+} to Eu^{3+} was also observed in other red-emitting phosphors $Na_{0.5}Sm_{0.1}Eu_{0.4}WO_4$ [12], $NaEu(MoO_4)_2$ [13] and other molybdate [14].

In this paper, we demonstrate energy transfer dynamical processes in YAG:Ce^{3+}, Pr^{3+} and $CaMoO_4:Sm^{3+}$, Eu^{3+} based on experimental measurements of photoluminescence (PL) and fluorescence decay curves.

2. Experimental

The powder samples have been prepared by conventional solid-state reaction. For the preparation of YAG:Ce^{3+}, Pr^{3+} phosphor, Y_2O_3, CeO_2, Al_2O_3 and Pr_6O_{11} are mixed in 1 M $(Y_{1-x-y}Ce_xPr_y)_3Al_5O_{12}$ (x, y represent the concentration of Ce^{3+} and Pr^{3+}, respectively) and 3 wt% BaF_2 was added as the flux. After a good mixing in an agate mortar, the mixture was sintered

* Corresponding author. Tel./fax: +86 431 86176317.
E-mail address: zhangjh@ciomp.ac.cn (J. Zhang).

0022-2313/$ - see front matter © 2010 Elsevier B.V. All rights reserved.
doi:10.1016/j.jlumin.2010.09.011

at 1500 °C for 3 h under a reducing atmosphere. $CaMoO_4:Sm^{3+}/Eu^{3+}$ phosphors were obtained by solid-state reaction in air as reported previously [10]. The structure of final products is characterized by power X-ray diffraction (XRD). PL spectra are measured with a Hitachi Spextra-fluorometer (F-4500). The decay of fluorescence with lifetime less than 1 μs is measured by an FL920 fluorometer (Edinburgh Instruments, Livingston, UK) with a hydrogen flash lamp (nF900; Edinburgh Instruments). In the measurements of fluorescent decay with lifetime longer than 1 μs, an optical parametric oscillator (OPO) is used as an excitation source. The signal is detected by a Tektronix digital oscilloscope (TDS 3052).

3. Results and discussion

3.1. Energy transfer in YAG:Ce^{3+}, Pr^{3+}

Fig. 1 shows the decay curve of yellow fluorescence of Ce^{3+} in sample series A $(Y_{0.99-x}Ce_{0.01}Pr_x)_3Al_5O_{12}$. The decay is measured by monitoring at 530 nm on 340 nm pulsed excitation. The decay changes from exponential to non-exponential patterns with increasing x, reflecting the effect of Ce^{3+}–Pr^{3+} ET. The ET pathway is conformably considered to start from the lowest 5d state of Ce^{3+} to the $^1D_2$ state of Pr^{3+}. Based on the Ce^{3+} and Pr^{3+} energy level diagrams, a radiative ET seems to be possible. However, we cannot observe the red line in a blend of YAG:Ce^{3+} and YAG:Pr^{3+} phosphors, indicating that ET takes place rather by non-radiative interaction, as suggested by Yang and Kim [6]. The normalized intensity of donor fluorescence can be written as

$$I_D(t) = I_{D0}(t) f(t) \quad (1)$$

where $I_{D0}(t)$ is the decay function of donors in the absence of acceptors and the function $f(t)$ characterizes loss of excited donors due to one way ET to the acceptors. If the ET rate between a donor and an acceptor is proportional to an inverse power of the distance r, written as α/r^m, according to the Inokuti–Hirayama [15] formula, we have

$$f(t) = \exp\left[-\frac{4}{3}\pi\Gamma\left(1-\frac{3}{m}\right)n_A\alpha^{3/m}t^{3/m}\right] \quad (2)$$

where α is a rate constant for ET; $m=6$, 8 and 10 are the coefficients for dipole–dipole, dipole–quadrupole, and quadrupole–quadrupole interaction, respectively and n_A is the number of acceptor ions per unit volume. From Eqs. (1) and (2), $\ln\{\ln[I_{D0}(t)/I_D(t)]\}$ acts as a linear function of $\ln(t)$ with a slope of $3/m$, and $\ln[I_D(t)/I_{D0}(t)]$ is proportional to $t^{3/m}$ with a slope of $4\pi\Gamma(1-3/m)n_A\alpha^{3/m}/3$. Labeling the 5d state of Ce^{3+} by 1, the log–log plot of $\ln[I_{10}(t)/I_1(t)]$ vs. t for sample $(Y_{0.99-x}Ce_{0.01}Pr_x)_3Al_5O_{12}$ with $x=0.02$ is presented in Fig. 2. It is demonstrated that the slope for $t>20$ ns is 0.56, close to 1/2, indicating an electric dipole–dipole interaction for ET. Regarding m as 6, we have plotted $\ln[I_1(t)/I_{10}(t)]$ vs. $t^{1/2}$ for the samples $(Y_{0.99-x}Ce_{0.01}Pr_x)_3Al_5O_{12}$ with $x=0.01$ and 0.02, as shown in Fig. 3. The best fitting to each of the two curves yields a transfer constant $\alpha=4.5\times10^{-36}$ cm^6s^{-1} for Ce^{3+}–Pr^{3+} ET in YAG with Ce^{3+} concentration of 0.01. In the fitting n_A, i.e. the number density of Pr^{3+}, is given by xN_Y with $N_Y=1.38\times10^{22}$ cm^{-3} being the number of Y sites per unit volume in YAG. Using the value of α the critical ET distance r_0 (the spatial separation between a donor and an acceptor, where the ET rate $\alpha/r_0^6=1/\tau_{10}$) is calculated to be about 0.81 nm. In the calculation, the intrinsic lifetime τ_{10} is 61 ns determined in 0.0005 Ce^{3+} lowly doped YAG, which exhibits a pure exponential decay. In Fig. 2 there is an increase in slope below 20 ns, forming a crossover [16]. As we know, Eq. (2) is obtained by assuming the

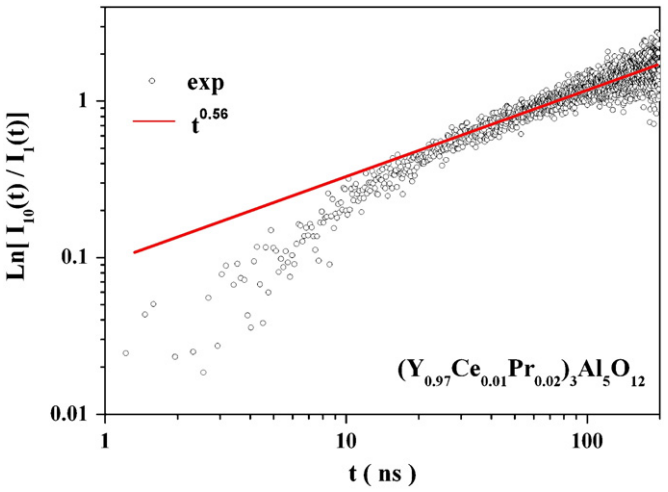

Fig. 2. log–log plot of $\ln[I_{10}(t)/I_1(t)]$ vs. t for sample $(Y_{0.99-x}Ce_{0.01}Pr_x)_3Al_5O_{12}$ with $x=0.02$. The solid line indicates the fitting behaviors.

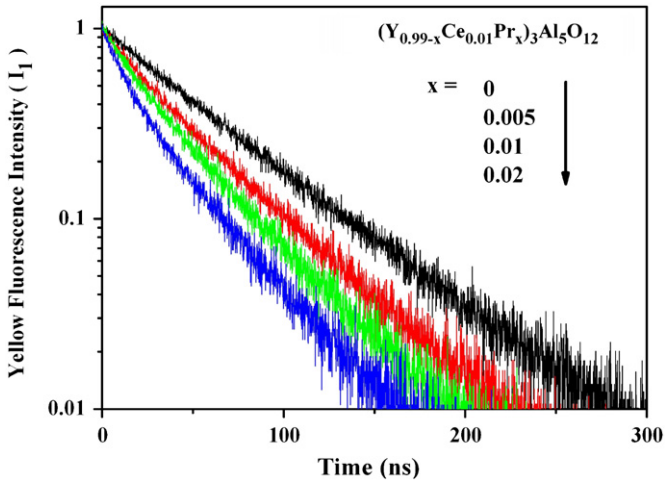

Fig. 1. Decay curves of yellow fluorescence in $(Y_{0.99-x}Ce_{0.01}Pr_x)_3Al_5O_{12}$ for $x=0$, 0.005, 0.01 and 0.02.

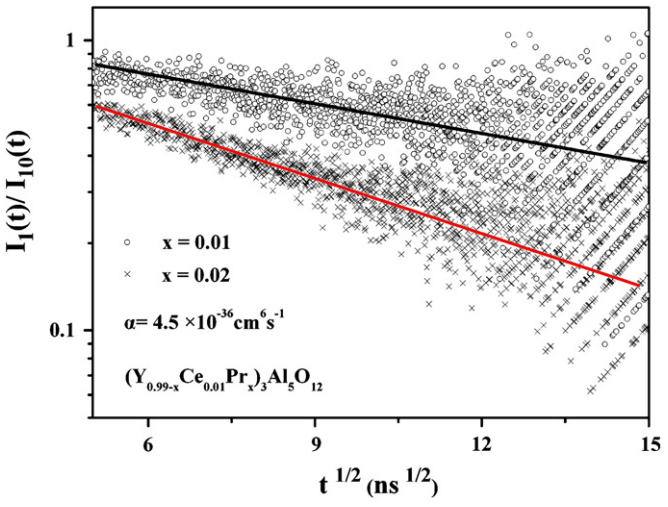

Fig. 3. Plotted $\ln[I_1(t)/I_{10}(t)]$ vs. $t^{1/2}$ for the samples $(Y_{0.99-x}Ce_{0.01}Pr_x)_3Al_5O_{12}$ with $x=0.01$ and 0.02. The solid line indicates the fitting behaviors.

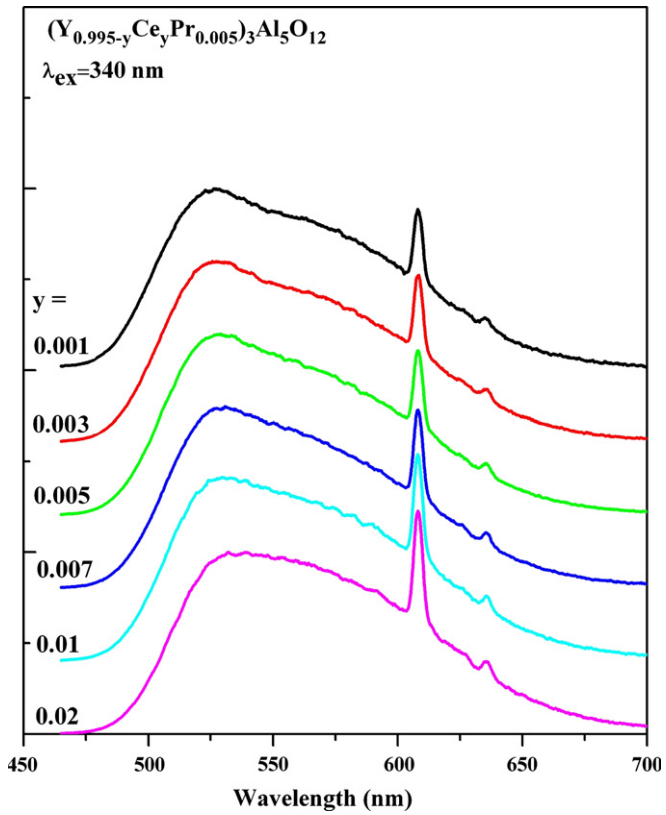

Fig. 4. PL spectra of $(Y_{0.095-y}Ce_yPr_{0.005})_3Al_5O_{12}$, ($y$=0–0.02) upon 340 nm excitation, where intensity of the yellow band in each spectrum is normalized.

nearest distance between a donor and a acceptor to be 0, leading to an infinite initial ET rate. Hence, Eq. (2) is not applicable at short times, which is less than 20 ns in the present sample.

To improve the color rendering of white LED, it was observed [5,6] that further increasing Pr^{3+} concentration for obtaining sufficient red componnets, however, leads to reduction of the red line due to Pr^{3+}–Pr^{3+} self-quenching [17,18]. Fig. 4 shows the PL spectra of sample series B $(Y_{0.995-y}Ce_yPr_{0.005})_3Al_5O_{12}$ with Pr^{3+} concentration fixed at 0.005 and various Ce^{3+} concentration y in the range 0–0.02, where intensity of the yellow emisson band of Ce^{3+} is normalized. It can be seen that the intensity ratio of red to yellow emission (R/Y) monotonously grows up with increasing y, showing a way to improve the red component of the phosphor. In view of small changes of the red fluorescence lifetimes with increasing y, the enhanced red line is an indication of increased macroscopic Ce^{3+}–Pr^{3+} ET rate. One can find the existence, in connection with the enhancement of the R/Y ratio, of a redshift of the yellow PL band with increasing Ce^{3+} concentration, as has been observed in Ce^{3+} singly doped YAG [19]. The redshift enhances the spectral distribution of the yellow band at the position of the red line. As a result, we suggest that the redshift is favourable for effectively increasing the spectral overlap integrals between the yellow emission band and the red absorption line, and therefore enhancing the ET rate. In the case of much narrower red line than the yellow band, their spectral overlap integral is proportional to the spectral intensity of the yellow band at the red line site, denoted by Y_R. The R/Y ratio and Y_R, approximately satisfy a proportional relationship, as shown in Fig. 5.

3.2. Energy transfer in $CaMoO_4$:Sm^{3+}, Eu^{3+}

The PL spectra of Sm^{3+} singly doped $CaMoO_4$ under excitation at 405 nm exhibit three characteristic transitions of Sm^{3+}:

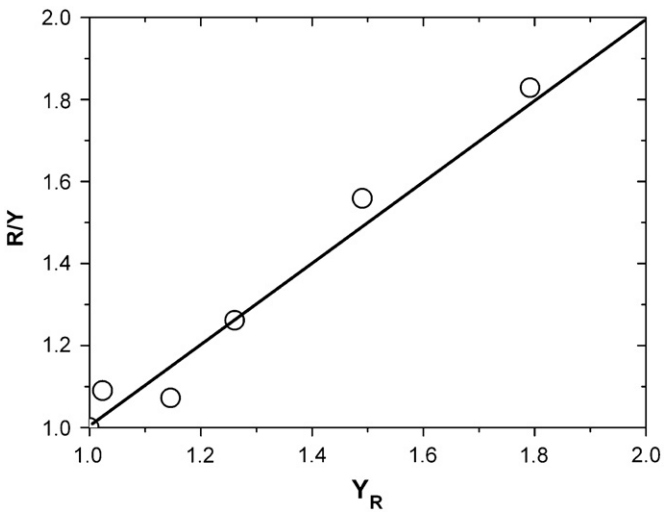

Fig. 5. Dependence of R/Y ratio on Y_R, where values of both R/Y and Y_R for the lowest y of 0.001 are normalized.

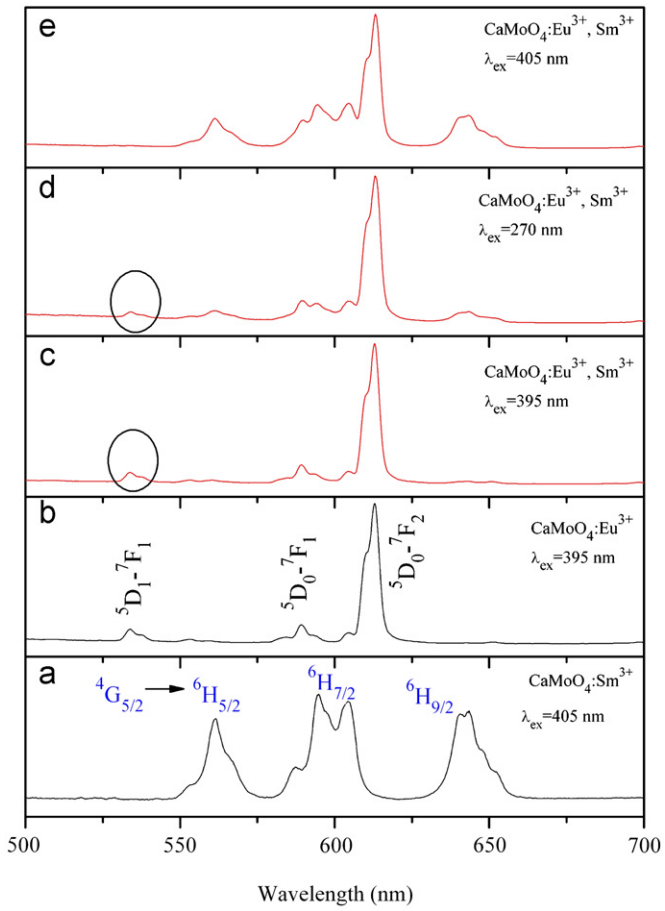

Fig. 6. Emission spectra of (a) $CaMoO_4:Sm^{3+}$ (λ_{ex}=405 nm), (b) $CaMoO_4:Eu^{3+}$ (λ_{ex}=395 nm), (c, d) $CaMoO_4:Eu^{3+}$, Sm^{3+} (λ_{ex}=395, 270 and 405 nm, respectively).

$^4G_{5/2}\rightarrow{}^6H_{5/2}$ (561 nm), $^4G_{5/2}\rightarrow{}^6H_{7/2}$ (596 nm, 604 nm) and $^4G_{5/2}\rightarrow{}^6H_{9/2}$ (642 nm), as shown in Fig. 6(a). The PL spectra of Eu^{3+} singly doped $CaMoO_4$ under excitation at 395 nm consist of series of characteristic lines of Eu^{3+} originating from the transitions of $^5D_1\rightarrow{}^7F_1$ at 534 nm, $^5D_0\rightarrow{}^7F_1$ at 590 nm and

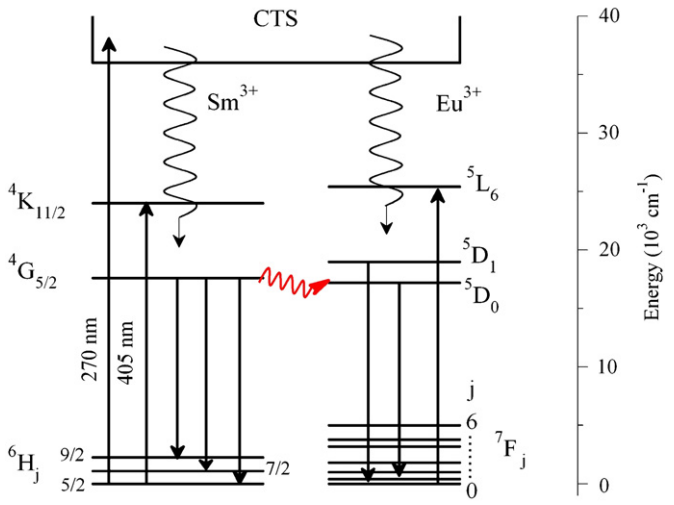

Fig. 7. Scheme of energy transfer pathway in $CaMoO_4$:Eu^{3+}, Sm^{3+}.

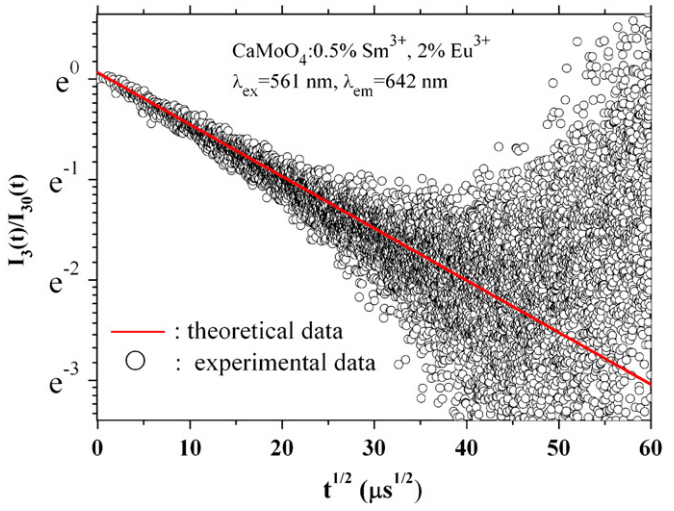

Fig. 8. Plotted $\ln[I_3(t)/I_{30}(t)]$ vs. $t^{1/2}$ for $CaMoO_4$: 0.5% Sm^{3+}, 2% Eu^{3+}. The solid line indicates the fitting behaviors.

$^5D_0 \rightarrow {}^7F_2$ at 612 nm as shown in Fig. 6(b). In Eu^{3+} and Sm^{3+} doubly doped $CaMoO_4$, the PL spectra under 395 nm excitation (see Fig. 6(c)) are the same as that of Eu^{3+} singly doped samples, indicating that Sm^{3+} cannot be excited by 395 nm and there is no energy transfer from Eu^{3+} to Sm^{3+}. When the doubly doped sample is excited at 270 nm, characteristic emissions of both Eu^{3+} and Sm^{3+} can be observed, as shown in Fig. 6(d). As the doubly doped sample is excited into the $^4K_{11/2}$ level of Sm^{3+} at 405 nm, besides the fluorescence of Sm^{3+}, the fluorescence from $^5D_0 \rightarrow {}^7F_1$ and $^5D_0 \rightarrow {}^7F_2$ transitions of Eu^{3+} is also observed (see Fig. 6(e)). This is the indication of energy transfer from Sm^{3+} to Eu^{3+}. A notable behavior presented in Fig. 6(e) is that the $^5D_1 \rightarrow {}^7F_1$ emission of Eu^{3+} disappears. As a result, the energy transfer pathway is from $^4G_{5/2}$ of Sm^{3+} to the $^5D_0$ of Eu^{3+} rather than $^5D_1$ level, as illustrated in the energy level diagram in Fig. 7.

To know the mechanism of energy transfer from the $^4G_{5/2}$ level of Sm^{3+} to $^5D_0$ level of Eu^{3+}, decay of $^4G_{5/2} \rightarrow {}^6H_{9/2}$ fluorescence $I_3(t)$ of Sm^{3+} is measured by monitoring at 642 nm while the $^4G_{5/2}$ level is excited at 561 nm in $CaMoO_4$: 0.5% Sm^{3+}, 2% Eu^{3+}. The ln–ln plot of $\ln[I_{30}(t)/I_3(t)]$ vs. t shows a slope close to 3/6, indicating an electric dipole–dipole energy transfer with $m=6$. Fig. 8 shows the plot of $\ln[I_3(t)/I_{30}(t)]$ vs. $t^{1/2}$. The slope of linear pattern yields α to be 8.5×10^{-40} cm^6 s^{-1}. The critical ET distance of 0.89 nm is evaluated. In the calculation, $I_{30}(t)$ has an exponential decay of the form $\exp(-t/\tau_{30})$, where τ_{30} is 595 μs as obtained in $CaMoO_4$: 0.5% Sm^{3+}.

4. Conclusion

Non-radiative energy transfers (ET) from Ce^{3+} to Pr^{3+}in $Y_3Al_5O_{12}$:Ce^{3+}, Pr^{3+} and from Sm^{3+} to Eu^{3+} in $CaMoO_4$:Sm^{3+}, Eu^{3+} are both governed by an electric dipole–dipole interaction. For Ce^{3+} concentration of 0.01, the corresponding rate constant and critical distance are evaluated to be 4.5×10^{-36} cm^6 s^{-1} and 0.81 nm, respectively, for Ce^{3+}–Pr^{3+} ET in YAG. An increase in red/yellow ratio on increasing Ce^{3+} concentration is observed. This behavior is attributed to the increase of spectral overlap integrals between Ce^{3+} emission and Pr^{3+} excitation due to the fact that the yellow band shifts to the red side with increasing Ce^{3+} concentration while the red line does not move.

In $CaMoO_4$:Sm^{3+}, Eu^{3+} phosphor, Sm^{3+}–Eu^{3+} transfer occurs from $^4G_{5/2}$ of Sm^{3+} to $^5D_0$ of Eu^{3+}. The transfer rate constant of 8.5×10^{-40} cm^6 s^{-1} and the critical transfer distance of 0.89 nm are evaluated.

Acknowledgments

This work was financially supported by the National Nature Science Foundation of China (10834006, 10774141, 10904141, 10904140), the MOST of China (2006CB601104), the Scientific project of Jilin province (20090134, 20090524) and CAS Innovation Program.

References

[1] G. Blasse, A. Bril., Appl. Phys. Lett. 11 (1967) 53.
[2] G. Blasse, A. Bril., J. Chem. Phys. 47 (12) (1967) 5139.
[3] R. Mueller-Mach, G.O. Mueller, M.R. Krames, T. Trottier, IEEE J. Sel.. Top. Quantum Electron. 8 (2002) 339.
[4] Y. Pan, M. Wu, Q. Su, J. Phys. Chem. Solids 65 (2004) 845.
[5] H.S. Jang, W.BinPlease check the second author's name in Ref. [5] as 'W.Bin' has been tagged as given name and 'Im' as surname.Correct if necessary. Im, D.C. Lee, D.Y. Jeon, S.S. Kim, J. Lumin. 126 (2007) 371.
[6] H. Yang, Y.S. Kim, J. Lumin. 128 (2008) 1570.
[7] H. Yang, D.K. Lee, Y.S. Kim, Mater. Chem.Phys. 114 (2009) 665.
[8] J.G. Wang, X.P. Jing, C.H. Yan, J.H. Lin, J. Electrochem. Soc. 152 (2005) G186.
[9] J. Liu, H.Z. Lian, C.S. Shi, Opt. Mater. 29 (2007) 1591.
[10] S.X. Yan, J.H. Zhang, X. Zhang, S.Z. Lu, X.G. Ren, Z.G. Nie, X.J. Wang, J. Phys. Chem. C 111 (2007) 13256.
[11] Y. Jin, J.H. Zhang, S.Z. Lu, H.F. Zhao, X. Zhang, X.J. Wang, J. Phys. Chem. C 112 (2008) 5860.
[12] W.W. Holloway Jr., M. Kestigian, J. Opt. Soc. Am. 56 (1966) 1171.
[13] Z. Wang, H. Liang, M. Gong, Q. Su, Electrochem. Solid-State Lett. 8 (2005) H33.
[14] X. Wang, Y. Xian, G. Wang, J. Shi, Q. Su, M. Gong, Opt. Mater. 30 (2007) 521.
[15] M. Inokuti, F. Hirayama, J. Chem. Phys. 43 (1965) 1978.
[16] P.M. Selzer, D.L. Huber, B.B. Barnett, W.M. Yen, Phys. Rev. B 17 (1978) 4979.
[17] M. Malinowski, P. Szczepanski, W. Woliński, R. Wolski, Z. Frukacz, J. Phys.: Condens. Matter 5 (1993) 6469.
[18] Houtong Chen, Rui Lian, Min Yin, Liren Lou, Weiping Zhang, Shangda Xia, Jean-Claude Krupa, J. Phys.: Condens. Matter 13 (2001) 1151.
[19] T.Y. Tien, E.F. Gibbons, R.G. Delosh, P.J. Zacmanidis, D.E. Smith, H.L. Stadler, J. Electrochem. Soc: Solid State Sci. Technol. 120 (1973) 278.